NANO LETTERS

pubs.acs.org/NanoLett Letter

2D Materials by Design: Intercalation of Cr or Mn between two VSe_2 van der Waals Layers

Vimukthi Pathirage, Salma Khatun, Sergey Lisenkov, Kinga Lasek, Jingfeng Li, Sadhu Kolekar, Manuel Valvidares, Pierluigi Gargiani, Yan Xin, Inna Ponomareva, and Matthias Batzill*

Cite This: *Nano Lett.* 2023, 23, 9579–9586 Read Online

ACCESS | Metrics & More | Article Recommendations | Supporting Information

ABSTRACT: Insertion of metal layers between layered transition-metal dichalcogenides (TMDs) enables the design of new pseudo-2D nanomaterials. The general premise is that various metal atoms may adopt energetically favorable intercalation sites between two TMD sheets. These covalently bound metals arrange in metastable configurations and thus enable the controlled synthesis of nanomaterials in a bottom-up approach. Here, this method is demonstrated by the insertion of Cr or Mn between VSe_2 layers. Vacuum-deposited transition metals diffuse between VSe_2 layers with increasing concentration, arranging in ordered phases. The Cr^{3+} or Mn^{2+} ions are in octahedral coordination and thus in a high-spin state. Measured and computed magnetic moments are high for dilute Cr atoms, but with increasing Cr concentration the average magnetic moment decreases, suggesting antiferromagnetic ordering between Cr ions. The many possible combinations of transition metals with TMDs form a library for exploring quantum phenomena in these nanomaterials.

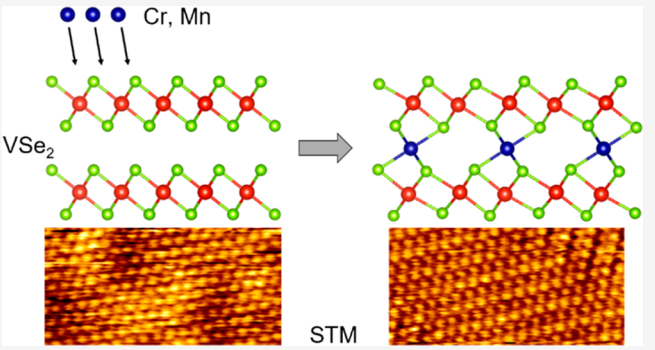

KEYWORDS: *2D materials, intercalation, surface science, materials modifications, molecular beam epitaxy*

Creating artificial van der Waals (vdW) materials by restacking 2D sheets on top of each other has been recognized as an opportunity for materials design.[1−3] Recently it has been proposed that a special class of non-vdW materials can also be isolated in pseudo-2D ultrathin crystals by exfoliation from bulk crystals[4,5] or grown as ultrathin films.[6] These non-vdW materials have in common that they exhibit a layered "backbone" structure that gives them a a preferred cleavage plane. These materials can be considered as a class of 2D sheets augmenting the existing family of 2D materials. Here we demonstrate a bottom-up synthesis approach that enables the synthesis of pseudo 2D crystals that may not have any bulk counterpart.

We focus on the modification of transition-metal dichalcogenides (TMDs) by insertion of transition metals (TM) between TMD layers. TMDs are a versatile family of 2D materials,[7] with many early-transition-metal chalcogenides also known to exhibit various ordered self-intercalation compounds,[8,9] illustrated in Figure 1. For different concentrations, in-plane ordered 2 × 2, $\sqrt{3} \times \sqrt{3}$ R30°, or 2 × 1 superstructures are known.[10] Previous studies of ultrathin pseudo 2D crystals of this class are based on known bulk phases or self-intercalation compounds (i.e., only one kind of TM).[10,11,14] Bulk-exfoliated sheets or thin films of these materials have demonstrated important phenomena, such as concentration-dependent magnetic anisotropy[6] and skyrmion lattices in $Cr_{1+\delta}Te_2$,[12,13] magnetic properties of self-intercalated TaS_2[14] and in VSe_2[15] and VTe_2,[16] proposed superconductivity in $Ni_{1+\delta}Te_2$,[17] layer-dependent magnetism in $CrCuSe_2$,[5] and demonstration of heteroepitaxy of $CuCr_2Te_4$.[18] In contrast to these reports, a novel synthesis approach is discussed here that enables incorporation of various TMs between TMD sheets. The methodology can be described by a two-step process: (i) synthesis of ultrathin TMD sheets and (ii) intercalation of TM between the TMD layers. The two separate steps enable control over the amount of inserted TM from dilute atoms to several ordered superstructures. Importantly, this approach is fundamentally different from synthesis methods that provide the constituent elements of the films simultaneously, e.g., by codeposition in molecular beam epitaxy (MBE). Under such conditions the elements can arrange in any structure with their preferred chalcogen concentration; this may, for instance, result in alloyed TMDs rather than an intercalation compound. In contrast, forming a TMD with a single TM first will define the chalcogen concentration and the TMD "backbone"

Received: August 22, 2023
Revised: October 5, 2023
Published: October 11, 2023

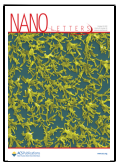

https://doi.org/10.1021/acs.nanolett.3c03169
Nano Lett. 2023, 23, 9579−9586

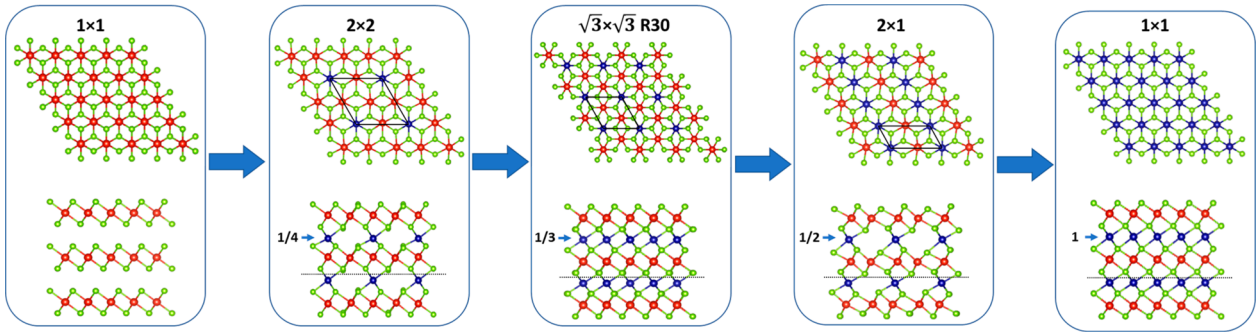

Figure 1. Illustration of the relationship between 1T-TMDs and various compounds with $TM_{1+\delta}X_2$ (TM = transition metal and X = chalcogen) compositions. The δ indicates the concentration of TM inserted between TMD layers. In the figure metal atoms in the TMD layer are illustrated as red, metal atoms in the interlayer region as blue, and chalcogen atoms as green circles. For $\delta = 1$, i.e., a completely filled inter-TMD-layer region, the NiAs structure is obtained. For lower concentrations of interlayer atoms, periodic in-plane superstructures with a 2×2, $\sqrt{3} \times \sqrt{3}$ R30, or 2×1 structure may be observed for $\delta = 1/4$, $1/3$, or $1/2$, respectively. The superstructures are indicated in the top-view images (top), and the cross-sectional views are shown at the bottom. The arrows illustrate the sequential increase in the amount of interlayer atoms.

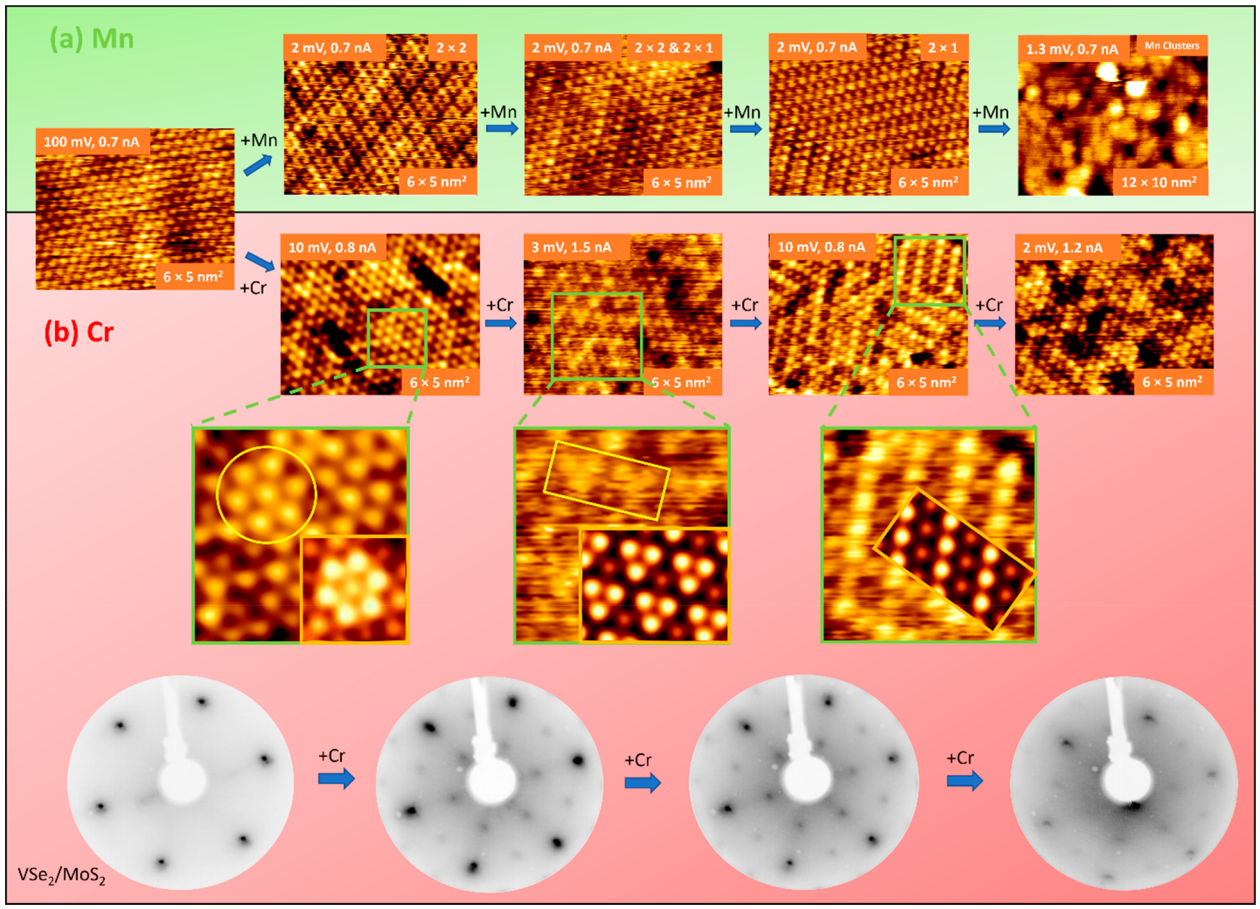

Figure 2. Scanning tunneling microscopy (STM) of bilayer VSe_2 with increasing Mn (a) and Cr insertion (b). For both elements formation of initially a 2×2 and then a 2×1 superstructure is observed, before the surface becomes disordered and eventually forms clusters at the surface. For Cr insertion the experimental STM images are also compared to simulated STM data for dilute amounts of Cr atoms, 1/4 monolayer (ML) of Cr atoms (2×2), and 1/2 ML of inserted Cr atoms (2×1). The simulated data are shown as insets in the zoomed-in experimental data. In addition to the STM, low-energy electron diffraction (LEED) has been conducted on another set of samples grown on single-crystalline MoS_2 substrates. With increasing Cr deposition, a transition from the 1×1 structure to a 2×2 diffraction pattern is observed. For low Cr concentrations the LEED pattern initially increases in "sharpness" before it becomes more diffuse, consistent with the STM data (note that we cannot distinguish a 2×1 structure with 3 rotational domains from a 2×2 superstructure).

structure. These TMD layers will act as the "scaffold-structure" for the subsequent low-temperature intercalation of the second TM. Here this approach is demonstrated for both Cr and Mn insertion into bilayer VSe_2.

Synthesis and Film Characterization. The growth of VSe_2 monolayers and few-layer samples by MBE has been reported previously.[19−22] In previous work it was demonstrated that insertion of V atoms between bilayers is possible

https://doi.org/10.1021/acs.nanolett.3c03169
Nano Lett. 2023, 23, 9579−9586

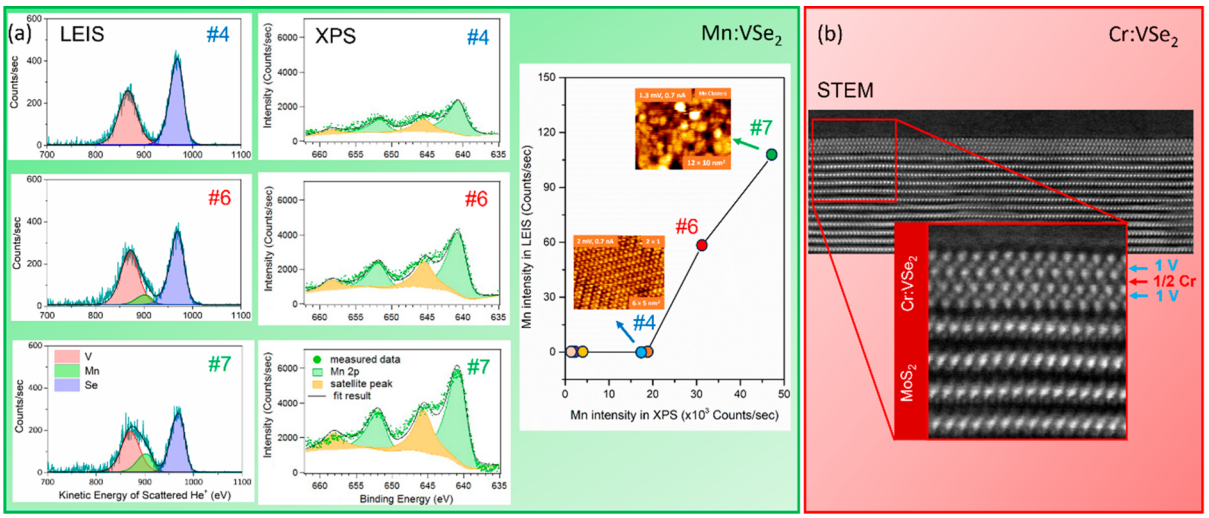

Figure 3. Determination of insertion of Mn (a) and Cr (b) in intercalation sites of bilayer VSe_2. LEIS and XPS measurements for sequential deposition of Mn on VSe_2 are shown in (a). XPS intensity increased with increasing Mn deposition, while an increase of the Mn peak intensity in LEIS is only observed after a threshold amount of Mn is deposited at roughly 1/2 ML, indicating that initially there is no Mn in the topmost surface layer and all Mn is incorporated subsurface. Additional information on the deconvolution of the LEIS spectra into V and Mn contributions is provided in Figure S5. The XPS peak shape exhibits a characteristic shakeup satellite (yellow) for Mn^{2+} throughout the deposition. STEM images of a bilayer VSe_2 grown on a MoS_2 substrate and subsequently modified by Cr adsorption are shown in (b). It demonstrates that the TMD structure is maintained but additional atoms are inserted between the TMD layers, as is illustrated by the line profiles in Figure S6. Quantitative EDS compositional analysis shown in Figure S6 confirms the Cr/V ratio in the epilayer to be that of $V_2Cr_{1/2}$.

by postgrowth vacuum annealing which eventually resulted in a 2 × 1 superstructure that is easily discerned by STM.[11] High-temperature growth may directly result in a 2 × 1 structure[23] with the insertion of V atoms between VSe_2 layers.[15] Figure S1 shows scanning tunneling microscopy (STM) images of bilayer VSe_2 without superstructure. Generally, avoiding the insertion of homoatoms in MBE-grown early-transition-metal TMDs is challenging, but low growth temperatures minimize the incorporation of homoatoms between TMD layers.[10]

To examine modifications of bilayer VSe_2, Cr or Mn atoms are sequentially deposited onto VSe_2 at ∼200 °C under an ultrahigh vacuum. STM images acquired after each deposition step do not show any disruption of the VSe_2 atomic lattice and or any indication of metal clusters at the surface. This illustrates that for bilayers small amounts of deposited Mn/Cr atoms diffuse subsurface. After the first deposition, some additional corrugation is observed with brighter atomic contrast for some surface Se atoms. Some protrusions may be identified by simulated STM images as single Cr atoms inserted between VSe_2 layers as indicated in Figure 2b. Generally, however, at a low concentration there exists significant disorder which prevents clear identification of isolated Cr atoms. With a further increase of the Mn/Cr concentration ordered superstructures are observed in STM, which can also be observed by low-energy electron diffraction (Figure 2 and Figure S4). This signals that the inserted Cr atoms are periodically arranged and cause a buckling and/or local electronic variation. Similar surface corrugation in STM has been reported for self-intercalated compounds.[6,10,11] For small Cr/Mn deposition a 2 × 2 superstructure is identified in good agreement with simulated STM images of 1/4 monolayer (ML) of Cr (here we define one ML as the amount of transition metal within a VSe_2 TMD layer). Further Mn/Cr addition results in a 2 × 1 structure, in agreement with simulated STM images for a 1/2 ML Cr. The simulated relaxed structures for the different compositions are given in Figure S2. Further Cr addition results in nonperiodic modulations. Finally, even more Mn/Cr causes surface roughening and Mn/Cr cluster formation (shown in Figure S3). In the experiments the critical Mn/Cr concentration for which surface clusters are formed is for approximately 1/2 ML of TM deposition.

The STM results are consistent with the TM inserted between the TMD layers and forming an intercalation compound. To verify that the deposited elements are diffusing subsurface, we conducted low-energy ion scattering spectroscopy (LEIS) with 1200 eV He^+ ions for Mn deposition on bilayer VSe_2. LEIS is an extreme surface-sensitive technique that probes the elemental composition of the topmost surface atoms.[24] Combining LEIS with X-ray photoemission spectroscopy (XPS), with the latter having a probing depth of ∼10 nm, we can compare the Mn concentration in the entire film with that in the top layer. LEIS and XPS measurements for increasing Mn concentration are shown in Figure 3a. Initially only the Mn XPS signal is increasing while no indication of Mn in LEIS is observed (see Figure S5 for additional spectra and LEIS peak fitting); only after an XPS intensity that corresponds to 1/2 ± 1/4 ML of Mn is reached do we also detect Mn in LEIS. This verifies that Mn is only present at the surface after a threshold coverage of ∼1/2 ML is reached.

For Cr insertion the LEIS studies are not possible because of the similar masses of Cr and V. Instead, we performed high-resolution scanning transmission electron microscopy (STEM) on a bilayer VSe_2 sample grown on a MoS_2 substrate. The sample was intercalated with Cr until a 2 × 1 superstructure was observed. The STEM data in Figure 3b show that the TMD structure is conserved but additional atoms are present between the TMD layers. Quantitative compositional analysis of the film by electron dispersive spectroscopy (EDS) finds a Cr/V atom ratio of 0.22, which is close to the ideal ratio of 0.25 for 1/2 ML of Cr sandwiched between two VSe_2 sheets (see Figure S6 for the EDS maps and compositional analysis).

https://doi.org/10.1021/acs.nanolett.3c03169
Nano Lett. 2023, 23, 9579−9586

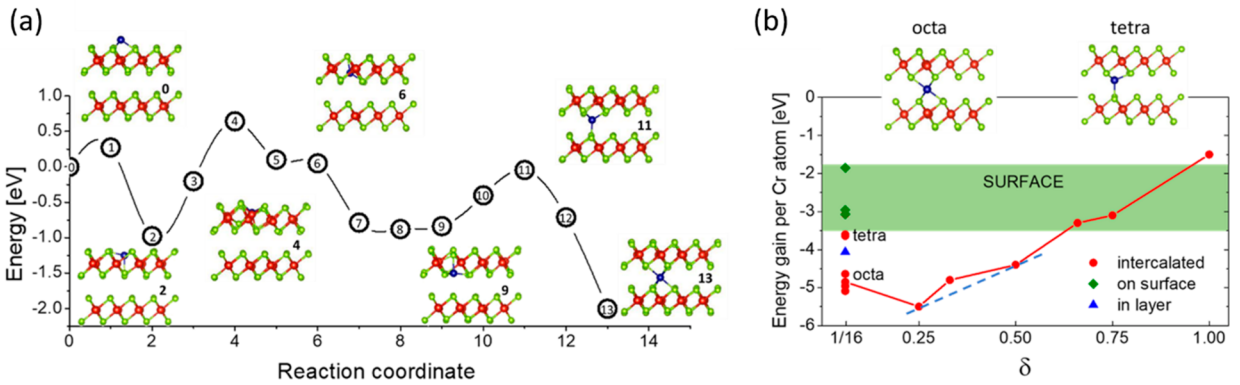

Figure 4. Energy evolution along the reaction path predicted in nudged elastic band calculations (a). Images 0 and 13 correspond to Cr adsorbed on the surface and inserted in an octahedral position, respectively. Energy gain for adsorption on the surface (green) or insertion between layers (red) as a function of Cr concentration δ (b). For δ = 1/16 several adsorption and insertion sites are identified from computations. They are associated with local minima on the energy surface. The insets illustrate the two high-symmetry octahedral and tetrahedral coordinations. We note that insertion sites that lie below octahedral sites yield structures with a slide between the layers and are not realized under our experimental conditions. The green band gives the energy range associated with surface adsorption. The blue symbol gives the energy for the local minimum when Cr resides inside the top layer. The energies for different ordered superstructures for their corresponding concentrations δ are shown as red dots and are connected to guide the eye. The dashed line indicates the tie line between the 2 × 2 and 2 × 1 structures. (Computational structures for the different concentrations are visualized in Figure S2). All computational structures are provided in https://github.com/USFmatscilab/VSe2-Cr.)

Thus, the experimental evidence indicates that Mn and Cr atoms can readily diffuse through the topmostVSe_2 layer and occupy interstitial sites in between VSe_2 layers. Moreover, the intercalation results in 2 × 2 and 2 × 1 superstructures, while a $\sqrt{3} \times \sqrt{3}$ R30° superstructure, which may be associated with a 1/3 ML Mn/Cr concentration, has not been observed in LEED or STM. To gain insight into these experimental observations, nudged elastic band technique within density functional theroy (DFT) simulations was used to assess the feasibility of vapor-deposited Cr atoms to reach the region between two VSe_2 layers. Figure 4a shows a diffusion path of a single Cr atom through a VSe_2 layer. In this case the VSe_2 bilayer remains in a 1T stacking: i.e., the two TMD layers are not allowed to translate relative to each other. Figure S7 shows calculations with this restriction removed, which leads to barrierless diffusion. For VSe_2 in a fixed 1T stacking, we find modest diffusion barriers that can be overcome at the Cr-deposition temperature of ∼200 °C. At this temperature the estimation based on transition state theory gives a hopping rate for Cr of 10^5−10^6 s^{-1} over the predicted 0.64 eV barrier. Once Cr is inserted between the layers the hopping rate to diffuse back to the surface is a negligible 10^{-15} s^{-1}. Importantly, the adsorption energy for Mn/Cr between the two VSe_2 layers is significantly lowered over the adsorption energy on the surface, as can be seen from Figure 4b (for Cr) and Figure S8 (for Mn). The calculations also confirm that an octahedral configuration between the VSe_2 layers is energetically preferred by 1.25 eV over the tetrahedral configuration.

With increasing Mn/Cr concentration different periodic Cr arrangements are possible (Figure 1). Keeping Mn/Cr at the octahedral sites, the insertion energies for Mn/Cr atoms in 2 × 2 (1/4 ML occupancy), $\sqrt{3} \times \sqrt{3}$ R30 (1/3 ML occupancy), 2 × 1 (1/2 ML occupancy) arrangements and occupancies with 2/3 and 3/4 are considered and the insertion energies per Cr atom are plotted in Figure 4b and for Mn in Figure S8. For δ =1/2 or less the computed energies are below the "green band" in the figure, indicating that the energy gain due to intercalation is greater than that due to adsorption on the surface. Interestingly a 2 × 2 ordered structure is lower in energy/atom than for Mn/Cr atoms farther apart. This indicates an attraction between inserted metal atoms and a preferred occupation of next-nearest-neighbor sites with twice the VSe_2 lattice spacing separation. With increasing Mn/Cr concentration, the energy benefits of inserting metal atoms into the gap become less. Importantly, the energy for the $\sqrt{3} \times \sqrt{3}$ R30° structure lies above a tie line between the energies for the 2 × 2 and 2 × 1 structures. This explains why the $\sqrt{3} \times \sqrt{3}$ R30° structure has not been observed in the experiments. Another important observation is that at Cr concentrations of ∼2/3 ML the insertion energies are within the green band, suggesting that insertion and adsorption become energetically competitive and both processes will coexist. This indicates a limit of the amount of metal atoms that can be inserted between VSe_2 layers, in agreement with the experiments.

Chemical Properties. The chemical integrity of VSe_2 and the charge state of the inserted Cr atoms is assessed by synchrotron X-ray absorption spectroscopy (XAS). The evolution of the V and Cr L edges are shown in Figure 5a,b. It is apparent that the line shape of the V L edge is not changing significantly for inserted Cr and only broadens once Cr adsorbs on the surface. A similar broadening of the V L edge of VSe_2 has been reported after Co and Fe adsorption on VSe_2 surfaces.[25,26]

The Cr L edge increases in intensity with increasing Cr deposition. Again, a notable change in the line shape occurs once Cr adsorbs on the surface, with a shoulder developing at higher photon energy. A similar Cr-surface species has also been observed in Cr-doped Bi_2Se_3.[27] Moreover, the line shape and energy position for the Cr insertion is like that of Cr-doped Bi_2Se_3, which was also associated with octahedrally coordinated Cr atoms (see Figure S9a). Another sensible comparison is to XAS spectra of Cr_2Se_3 (Figure S9b),[28] a compound with a similar structure. The Cr L edge is similar to these reference data, indicating octahedral coordination of the Cr atoms in a Cr^{3+} charge state. For thick Cr films (3 ML) the XAS is consistent with that of metallic Cr, indicating metal clusters at the surface. The charge state can be further justified by calculating the branching ratio, which is given by the

https://doi.org/10.1021/acs.nanolett.3c03169
Nano Lett. 2023, 23, 9579−9586

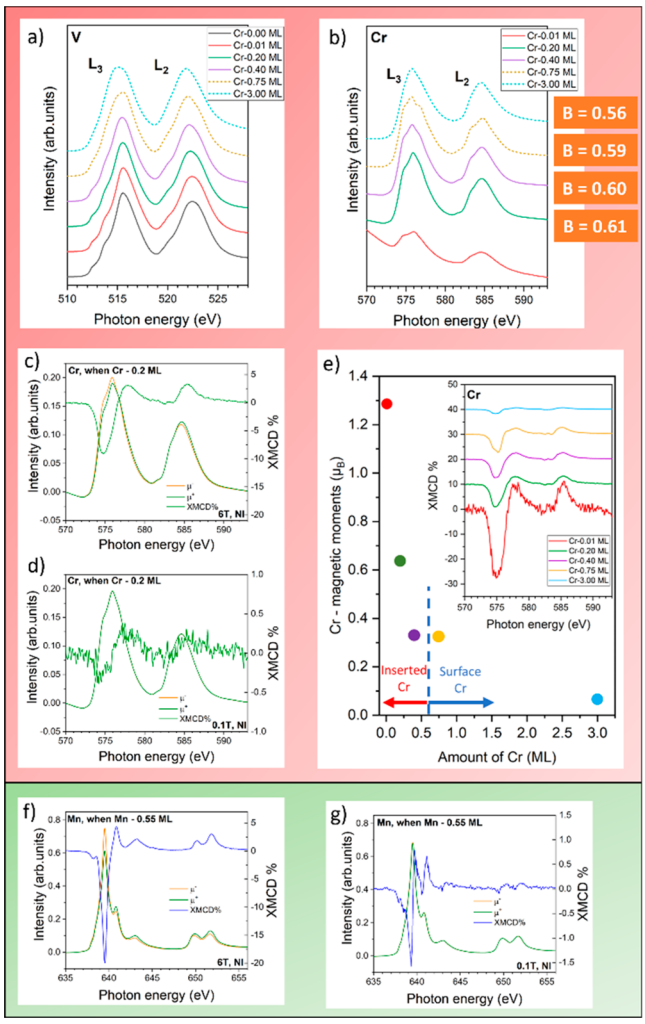

Figure 5. X-ray absorption (XAS) and X-ray magnetic circular dichroism (XMCD) spectroscopy of bilayer VSe_2 modified with Cr or Mn. (a) XAS for the V $L_{2,3}$ absorption edge. It demonstrates the chemical integrity of VSe_2 as Cr is being deposited. The solid lines indicate spectra with Cr expected to be mostly inserted between the VSe_2 layers, while dashed lines are for spectra on samples for which the deposited Cr amount exceeds the amount of Cr that can be incorporated between VSe_2 layers. The VSe_2 spectra remain almost unchanged and only broaden once the Cr amount exceeds the amount that can be inserted between the layers. (b) Corresponding Cr $L_{2,3}$ absorption edge for the same samples as in (a). Again, the Cr spectra change little (apart from intensity) with increasing Cr deposition as long as the Cr is inserted between the VSe_2 layers. Once Cr adsorbs on the surface, an additional component is observed (indicated by an arrow). For thick films (3 ML) the spectrum resembles that of metallic Cr. The branching ratio B is also indicated for each spectrum. Cr L-edge XMCD spectra for 0.2 ML Cr inserted in VSe_2 are shown (c) in a 6 T applied field and (d) in a 0.1 T field. The average magnetic moment per Cr atom as a function of intercalated Cr is shown in (e) with the inset indicating the measured XMCD signal. The Mn L edge XMCD for the 6 T applied field is shown in (f) and at low field (0.1 T) in (g). Note the different scale for the XMCD signal.

intensity ratio of the L_2 and L_3 excitations and is calculated as $B = I(L3)/[I(L3) + I(L2)]$. For Cr in an octahedral crystal field ($10Dq$ = 1.5 eV)[29] the branching ratio is expected to be B = 0.593 for Cr^{3+} ($3d^3$) and B = 0.672 for Cr^{2+} ($3d^4$). The ratios for samples with Cr inserted between VSe_2 are close to 0.6 (Figure 5b), indicating that Cr is in a $3d^3$ state. For the thick film, Cr is metallic and thus the branching ratio is very different (B = 0.56). At first glance a Cr^{3+} charge state with vanadium maintaining a V^{4+} charge state appears to violate charge neutrality. However, this is consistent with previous measurements of self-intercalated VSe_2.[11] In that case, high-resolution XPS showed that the charge state of V is not significantly altered by introduction of V atoms but that Se core levels are exhibiting a chemical shift, suggesting a change in the chalcogen charge state.

Cr ions in a $3d^3$ electronic configuration and in an octahedral crystal field suggests a high-spin state from crystal field theory. A high spin of 2.6 μ_B is also computed by DFT, which gives further support for a Cr $3d^3$ state. Experimentally the magnetic properties have been investigated by X-ray magnetic circular dichroism (XMCD), discussed next.

Magnetic Properties. Pristine VSe_2 is paramagnetic.[20,30] However, defects[31,32] and self-intercalated V[15] in VSe_2 have been shown to induce weak ferromagnetic properties. Consistent with these reports, the as-grown bilayer VSe_2 only exhibits a small magnetic moment in a 6 T magnetic field at a temperature of 4 K. Moreover, the weak vanadium XMCD signal decreases further (see Figure S10) with Cr insertion. In contrast, inserted Cr atoms exhibit a significant average magnetic moment at high field (6 T) but negligible magnetization (less than 0.5% of the XAS signal) at low field (0.1 T), as shown in Figure 5c,d for 0.2 ML Cr concentration and for other concentrations in Figure S11. The average magnetic moments per Cr atom in a 6 T applied field is calculated from the XMCD spectra using the sum rule and plotted in Figure 5e as a function of Cr concentration. The strongest XMCD signal is observed for very small amounts of Cr with a magnetic moment of ~1.4 μ_B. With increasing Cr insertion, the average magnetic moment per Cr atom decreases. This decrease may suggest that certain structural configurations have different exchange interactions possibly related to the different ordered structures. The decrease of the magnetic moments of the inserted Cr atoms with increasing Cr concentration may indicate antiferromagnetic ordering, and the measured average magnetic moment may be related to defects and structural domain boundaries in the Cr arrangements. It is known that the magnetic exchange interaction depends sensitively on the Cr−Cr separation in Cr chalcogenides; for instance, Cr_2Se_3 is antiferromagnetic[33] while Cr_2Te_3 is ferromagnetic.[34] The similar lattice constants of VSe_2 and $CrSe_2$ may thus support an antiferromagnetic ordering. Similar magnetic behavior is also observed for Mn intercalation. The XAS and XMCD spectra for ~0.5 ML inserted Mn are shown in Figure 5f,g for high and low applied magnetic fields, respectively. XAS indicates that the inserted Mn is in a 2+ charge state (also consistent with the XPS spectra shown in Figure 3 that exhibit the characteristic shake-up satellite structure for Mn^{2+}) and the measured magnetic moment in a 6 T applied field is ~0.4 μ_B (using a spin correction factor of 1 for Mn). In a low applied field (0.1 T) the average magnetic moment is very small.

For Cr, the magnetic moments have been verified by DFT calculations. In computations the magnetic moment only varies between 2.4−2.8 μ_B per atom for dilute Cr or Cr in different periodic structures. Such a magnetic moment is consistent with Cr being in a high-spin state and is comparable with the computational value of 2.7 μ_B for the antiferromagnetic $Im\bar{3}m$ Cr.[35] The fact that the magnetic moment per atom is not

https://doi.org/10.1021/acs.nanolett.3c03169
Nano Lett. 2023, 23, 9579−9586

changed significantly with increasing Cr content in the computation also supports the notion that the decreased average magnetic moment in the measurements must be due to antiferromagnetic exchange interactions of the Cr atoms. To further assess the exchange interactions of Cr in the 2 × 2 and 2 × 1 structures the energies for different spin configurations are calculated and the difference between the lowest energy antiferromagnetic configuration and the ferromagnetic configuration is shown in Figure S12. These calculations predict that 2 × 2 and $\sqrt{3} \times \sqrt{3}$ R30° exhibit a tendency to arrange ferromagnetically, while a 2 × 1 structure is indeed antiferromagnetic. The associated average magnetic moments are 2.5, 2.6, and 0 μ_B. These larger average magnetic moments compared to those in experiment may be explained by disorder in the Cr layer and a larger fraction ordering in the antiferromagnetic 2 × 1 structure. Moreover, more complex spin textures may develop,[36] especially in a single-atom 2D sheet, and this warrants further investigation.

While Cr and Mn inserted into VSe_2 have large magnetic moments, they appear antiferromagnetically ordered. Previous studies on pure VSe_2 have shown that ferromagnetic ordering can be induced by proximity with a ferromagnetic layer.[25,26] Similar proximity-induced ferromagnetic properties are also observed in the Cr:VSe_2 structure when a metallic ferromagnet (iron) is deposited onto the Cr:VSe_2 film. The element-specific XMCD hysteresis loops show that both Cr and V become ferromagnetically ordered, with their magnetic moments aligned antiparallel to that of the iron film (see Figure S13). This demonstrates potential for the Cr:VSe_2 structure for implementation in magnetic van der Waals heterostructures.

In conclusion, insertion of transition metals between TMD layers opens a new approach for designing vdW materials. For bulk TMD materials, doping by transition-metal insertion has been used to induce new functionalities, e.g., Cu doping of $TiSe_2$ to induce superconductivity.[37] In addition intercalated magnetic elements in TMD bulk crystals, which may be exfoliated as thin layers, have attracted interest for spintronics applications.[38] The approach demonstrated here enables precise control over the amount of inserted TM from single dispersed atoms to ordered superstructures. The low processing temperatures imply that metastable phases are accessible; i.e., while inserted TM between TMD layers may be energetically favored over other adsorption sites in the material, it may not be the global minimum for the element combination. Synthesis of metastable phases enables the design of new materials that are not accessible by exfoliation from bulk crystals. For instance, the Cr/Mn:VSe_2 system studied here is not a known bulk phase. While it is anticipated that this process is applicable for a wide range of TM and TMDs (especially the early-transition-metal dichalcogenides with octahedral TM coordination), future studies will need to explore the vast parameter space of TMDs and the insertion of possible TMs. Others are also actively searching by computational screening for magnetic materials[39] in this kind of compound, and the synthesis approach discussed here will enable testing of these predictions.

■ ASSOCIATED CONTENT

Supporting Information

The Supporting Information is available free of charge at https://pubs.acs.org/doi/10.1021/acs.nanolett.3c03169.

STM characterization of VSe_2 mono- and bilayer films, DFT structure of Cr-inserted VSe_2, STM characterization for excess of 0.7 ML of Cr, LEED measurements for Cr:VSe_2 as a function of Cr concentration, peak fitting of LEIS and Mn-concentration-dependent measurements, compositional analysis of Cr:VSe_2 by STEM-EDS, nudged elastic band calculations for Cr diffusion through bilayer VSe_2 allowing lateral relaxation and translation of the VSe_2 layers, DFT calculations of adsorption energy of Mn atoms on bilayer VSe_2, comparison of Cr line shapes with published data of related compounds, vanadium $L_{2,3}$ XAS and XMCD as a function of Cr insertion, chromium $L_{2,3}$ XMCD as a function of Cr insertion, DFT calculations of magnetic ordering in Cr:VSe_2, XMCD for proximity induced ferromagnetic ordering in Cr:VSe_2, and experimental and computational methods (PDF)

■ AUTHOR INFORMATION

Corresponding Author

Matthias Batzill − *Department of Physics, University of South Florida, Tampa, Florida 33647, United States;* orcid.org/0000-0001-8984-8427; Email: mbatzill@usf.edu

Authors

Vimukthi Pathirage − *Department of Physics, University of South Florida, Tampa, Florida 33647, United States*

Salma Khatun − *Department of Physics, University of South Florida, Tampa, Florida 33647, United States*

Sergey Lisenkov − *Department of Physics, University of South Florida, Tampa, Florida 33647, United States*

Kinga Lasek − *Department of Physics, University of South Florida, Tampa, Florida 33647, United States*

Jingfeng Li − *Department of Physics, University of South Florida, Tampa, Florida 33647, United States;* Present Address: Songshan Lake Materials Laboratory, Dongguan, Guangdong 523808, People's Republic of China

Sadhu Kolekar − *Department of Physics, University of South Florida, Tampa, Florida 33647, United States;* Present Address: Center for Materials for Electronics Technology, Pune 411008, India.

Manuel Valvidares − *ALBA Synchrotron Light Source, E-08290 Barcelona, Spain;* orcid.org/0000-0003-4895-8114

Pierluigi Gargiani − *ALBA Synchrotron Light Source, E-08290 Barcelona, Spain;* orcid.org/0000-0002-6649-0538

Yan Xin − *National High Magnetic Field Laboratory, Florida State University, Tallahassee, Florida 32310, United States*

Inna Ponomareva − *Department of Physics, University of South Florida, Tampa, Florida 33647, United States;* orcid.org/0000-0001-8937-4401

Complete contact information is available at: https://pubs.acs.org/10.1021/acs.nanolett.3c03169

Notes

The authors declare no competing financial interest.

■ ACKNOWLEDGMENTS

Financial support from the National Science Foundation under award DMR 2118414 is acknowledged. Computational work was supported by the U.S. Department of Energy, Office of

Basic Energy Sciences, Division of Materials Sciences and Engineering, under grant DE-SC0005245 and used resources of the National Energy Research Scientific Computing Center (NERSC), a U.S. Department of Energy Office of Science User Facility located at Lawrence Berkeley National Laboratory, operated under Contract No. DE-AC02-05CH11231 using NERSC award BES-ERCAP-0025236. The XAS/XMCD studies were performed at the BOREAS beamline at ALBA synchrotron under proposal 2022025647. M.V. and P.G. acknowledge funding by grants PID2020-116181RB-C32 and FlagEra SOgraphMEM PCI2019-111908-2 (AEI/FEDER). STEM characterization was performed at the National High Magnetic Field Laboratory, which is supported by National Science Foundation Cooperative Agreement No. DMR-21285569 and the State of Florida.

REFERENCES

(1) Geim, A. K.; Grigorieva, I. V. Van der Waals heterostructures. *Nature* **2013**, *499*, 419−425.
(2) Novoselov, K. S.; Mishchenko, A.; Carvalho, A.; Castro Neto, A. H. 2D materials and van der Waals heterostructures. *Science* **2016**, *353*, 461.
(3) Castellanos-Gomez, A.; Duan, X.; Fei, Z.; Gutierrez, H. R.; Huang, Y.; Huang, X.; Quereda, J.; Qian, Q.; Sutter, E.; Sutter, P. Van der Waals heterostructures. *Nat. Rev. Meth. Primers* **2022**, *2*, 58.
(4) Puthirath Balan, A.; Radhakrishnan, S.; Woellner, C. F.; Sinha, S. K.; Deng, L.; Reyes, C. d. l.; Rao, B. M.; Paulose, M.; Neupane, R.; Apte, A.; Kochat, V.; Vajtai, R.; Harutyunyan, A. R.; Chu, C.-W.; Costin, G.; Galvao, D. S.; Marti, A. A.; van Aken, P. A.; Varghese, O. K.; Tiwary, C. S.; Malie Madom Ramaswamy Iyer, A.; Ajayan, P. M. Exfoliation of a non-van der Waals material from iron ore hematite. *Nat. Nanotechnol.* **2018**, *13*, 602−609.
(5) Peng, J.; Su, Y.; Lv, H.; Wu, J.; Liu, Y.; Wang, M.; Zhao, J.; Guo, Y.; Wu, X.; Xie, Y.; et al. Even-odd-layer-dependent Ferromagnetism in Two-dimensional Non-van der Waals $CuCrSe_2$. *Adv. Mater.* **2023**, *35*, 2209365.
(6) Lasek, K.; Coelho, P. M.; Gargiani, P.; Valvidares, M.; Mohseni, K.; Meyerheim, H. L.; Kostanovskiy, I.; Zberecki, K.; Batzill, M. Van der Waals epitaxy growth of 2D ferromagnetic $Cr_{(1+\delta)}Te_2$ nanolayers with concentration-tunable magnetic anisotropy. *Appl. Phys. Rev.* **2022**, *9*, 011409.
(7) Lasek, K.; Li, J.; Kolekar, S.; Coelho, P. M.; Zhang, M.; Wang, Z.; Batzill, M.; et al. Synthesis and characterization of 2D transition metal dichalcogenides: Recent progress from a vacuum surface science perspective. *Surf. Sci. Rep.* **2021**, *76*, 100523.
(8) Ueda, Y.; Ohtani, T. Mechanochemical synthesis, vacancy-ordered structures and low-dimensional properties of transition metal chalcogenides. In *Handbook of Solid State Chemistry*, 1st ed.; Dronskowski, R., Kikkawa, S., Stein, A., Eds.; Wiley-VCH: 2017..
(9) Hayashi, A.; Imada, K.; Inoue, K.; Ueda, Y.; Kosuge, K. Phase diagram of $(M'_xM_{1-x})_3Se_4$ $(0 < x < 1)$ (M, M' = 3d-transition metal). *Bull. Inst. Chem. Res., Kyoto Univ.* **1986**, *64*, 186−206.
(10) Lasek, K.; Coelho, P. M.; Zberecki, K.; Xin, Y.; Kolekar, S.; Li, J.; Batzill, M. Synthesis of early transition metal tellurides (Ti-, V-, and Cr-telluride) by molecular beam epitaxy: From monolayer ditellurides to multilayer self-intercalation compounds. *ACS Nano* **2020**, *14*, 8473−8484.
(11) Bonilla, M.; Kolekar, S.; Li, J.; Xin, Y.; Coelho, P. M.; Lasek, K.; Zberecki, K.; Lizzit, D.; Tosi, E.; Lacovig, P.; Lizzit, S.; Batzill, M. Compositional phase change of early transition metal diselenide (VSe_2 and $TiSe_2$) ultrathin films by postgrowth annealing. *Adv. Mater. Interface* **2020**, *7*, 2000497.
(12) Saha, R.; Meyerheim, H. L.; Göbel, B.; Hazra, B. K.; Deniz, H.; Mohseni, K.; Antonov, V.; Ernst, A.; Knyazev, D.; Bedoya-Pinto, A.; Mertig, I.; Parkin, S. S. P. Observation of Néel-type skyrmions in acentric self-intercalated $Cr_{1+\delta}Te_2$. *Nat. Commun.* **2022**, *13*, 3965.
(13) Zhang, C.; Liu, C.; Zhang, J.; Yuan, Y.; Wen, Y.; Li, Y.; Zheng, D.; Zhang, Q.; Hou, Z.; Yin, G.; Liu, L.; Peng, Y.; Zhang, X.-X. Room-temperature magnetic skyrmions and large topological hall effect in chromium telluride engineered by self-intercalation. *Adv. Mater.* **2023**, *35*, 2205967.
(14) Zhao, X.; Song, P.; Wang, C.; Riis-Jensen, A. C.; Fu, W.; Deng, Y.; Wan, D.; Kang, L.; Ning, S.; Dan, J.; Venkatesan, T.; Liu, Z.; Zhou, W.; Thygesen, K. S.; Luo, X.; Pennycook, S. J.; Loh, K. P. Engineering covalently bonded 2D layered materials by self-intercalation. *Nature* **2020**, *581*, 171−177.
(15) Nakano, M.; Wang, Y.; Yoshida, S.; Matsuoka, H.; Majima, Y.; Ikeda, K.; Hirata, Y.; Takeda, Y.; Wadati, H.; Kohama, Y.; Ohigashi, Y.; Sakano, M.; Ishizaka, K.; Iwasa, Y. Intrinsic 2D ferromagnetism in V_5Se_8 epitaxial thin films. *Nano Lett.* **2019**, *19*, 8806.
(16) Guzman, R.; Ning, S.; Zhang, R.; Liu, H.; Ma, Y.; Zhang, Y.-Y.; Bao, L.; Yang, H.; Du, S.; Bosman, M.; Pennycook, S. J.; Gao, H.-J.; Zhou, W. Collective Magnetic Behavior in Vanadium Telluride Induced by Self-Intercalation. *ACS Nano* **2023**, *17*, 2450−2459.
(17) Pan, S.; Hong, M.; Zhu, L.; Quan, W.; Zhang, Z.; Huan, Y.; Yang, P.; Cui, F.; Zhou, F.; Hu, J.; Zheng, F.; Zhang, Y. On-site synthesis and characterizations of atomically-thin nickel tellurides with versatile stoichiometric phases through self-intercalation. *ACS Nano* **2022**, *16*, 11444−11454.
(18) Wang, H.; Wen, Y.; Zhao, X.; Cheng, R.; Yin, L.; Zhai, B.; Jiang, J.; Li, Z.; Liu, C.; Wu, F.; He, J. Heteroepitaxy of two-dimensional $CuCr_2Te_4$ with Robust Room-temperature Ferromagnetism. *Adv. Mater.* **2023**, *35*, 2211388.
(19) Bonilla, M.; Kolekar, S.; Ma, Y.; Diaz, H. C.; Kalappattil, V.; Das, R.; Eggers, T.; Gutierrez, H. R.; Phan, M.-H.; Batzill, M. Strong room-temperature ferromagnetism in VSe_2 monolayers on van der Waals substrates. *Nat. Nanotechnol.* **2018**, *13*, 289−293.
(20) Feng, J.; Biswas, D.; Rajan, A.; Watson, M. D.; Mazzola, F.; Clark, O. J.; Underwood, K.; Marković, I.; McLaren, M.; Hunter, A.; Burn, D. M.; Duffy, L. B.; Barua, S.; Balakrishnan, G.; Bertran, F.; Le Fèvre, P.; Kim, T. K.; van der Laan, G.; Hesjedal, T.; Wahl, P.; King, P. D. C. Electronic structure and enhanced charge-density wave order of monolayer VSe_2. *Nano Lett.* **2018**, *18*, 4493−4499.
(21) Duvjir, G.; Choi, B. K.; Jang, I.; Ulstrup, S.; Kang, S.; Ly, T. T.; Kim, S.; Choi, Y. H.; Jozwiak, C.; Bostwick, A.; Rotenberg, E.; Park, J.-G.; Sankar, R.; Kim, K.-S.; Kim, J.; Chang, Y. J. Emergence of a metal−insulator transition and high-temperature charge-density waves in VSe_2 at the monolayer limit. *Nano Lett.* **2018**, *18*, 5432−5438.
(22) Chua, R.; Henke, J.; Saha, S.; Huang, Y.; Gou, J.; He, X.; Das, T.; van Wezel, J.; Soumyanarayanan, A.; Wee, A. T. S. Coexisting charge-ordered states with distinct driving mechanisms in monolayer VSe_2. *ACS Nano* **2022**, *16*, 783−791.
(23) Chen, G.; Howard, S. T.; Maghirang, A. B., III; Cong, K. N.; Villaos, R. A. B.; Feng, L.-Y.; Cai, K.; Ganguli, S. C.; Swiech, W.; Morosan, E.; Oleynik, I. I.; Chuang, F.-C.; Lin, H.; Madhavan, V. Correlating structural, electronic, and magnetic properties of epitaxial VSe_2 thin films. *Phys. Rev. B* **2020**, *102*, 115149.
(24) Brongersma, H. H.; Draxler, M.; de Ridder, M.; Bauer, P. Surface composition analysis by low-energy ion scattering. *Surf. Sci. Rep.* **2007**, *62* (62), 63−109.
(25) Zhang, W.; Zhang, L.; Wong, P. K. J.; Yuan, J.; Vinai, G.; Torelli, P.; van der Laan, G.; Feng, Y. P.; Wee, A. T. S. Magnetic transition in monolayer VSe_2 via interface hybridization. *ACS Nano* **2019**, *13*, 8997−9004.
(26) Vinai, G.; Bigi, C.; Rajan, A.; Watson, M. D.; Lee, T.-L.; Mazzola, F.; Modesti, S.; Barua, S.; Ciomaga, M.; Hatnean; Balakrishnan, G.; King, P. D. C.; Torelli, P.; Rossi, G.; Panaccione, G.; et al. Proximity-induced ferromagnetism and chemical reactivity in few-layer VSe_2 heterostructures. *Phys. Rev. B* **2020**, *101*, 035404.
(27) Figueroa, A. I.; van der Laan, G.; Collins-McIntyre, L. J.; Zhang, S. L.; Baker, A. A.; Harrison, S. E.; Schönherr, P.; Cibin, G.; Hesjedal, T. Magnetic Cr doping of Bi_2Se_3: Evidence for divalent Cr from x-ray spectroscopy. *Phys. Rev. B* **2014**, *90*, 134402.
(28) Liu, M.; Huang, Y. L.; Gou, J.; Liang, Q.; Chua, R.; Arramel; Duan, S.; Zhang, L.; Cai, L. L.; Yu, X.; Zhong, D.; Zhang, W.; Wee, A.

https://doi.org/10.1021/acs.nanolett.3c03169
Nano Lett. 2023, 23, 9579−9586

T. S. Diverse structures and magnetic properties in nonlayered monolayer chromium selenide. *J. Phys. Chem. Lett.* **2021**, *12*, 7752−7760.
(29) Thole, B. T.; van der Laan, G. Branching ratio in x-ray absorption spectroscopy. *Phys. Rev. B* **1988**, *38*, 3158.
(30) Coelho, P. M.; Cong, K. N.; Bonilla, M.; Kolekar, S.; Phan, M.-H.; Avila, J.; Asensio, M. C.; Oleynik, I. I.; Batzill, M. Charge density wave state suppresses ferromagnetic ordering in VSe_2 monolayers. *J. Phys. Chem. C* **2019**, *123*, 14089−14096.
(31) Chua, R.; Yang, J.; He, X.; Yu, X.; Yu, W.; Bussolotti, F.; Wong, P. K. J.; Loh, K. P.; Breese, M. B. H.; Goh, K. E. J.; Huang, Y. L.; Wee, A. T. S. Can reconstructed Se-deficient line defects in monolayer VSe_2 induce magnetism? *Adv. Mater.* **2020**, *32*, 2000693.
(32) Yu, W.; Li, J.; Herng, T. S.; Wang, Z.; Zhao, X.; Chi, X.; Fu, W.; Abdelwahab, I.; Zhou, J.; Dan, J.; Chen, Z.; Chen, Z.; Li, Z.; Lu, J.; Pennycook, S. J.; Feng, Y. P.; Ding, J.; Loh, K. P. Chemically exfoliated VSe_2 monolayers with room-temperature ferromagnetism. *Adv. Mater.* **2019**, *31*, 1903779.
(33) Adachi, Y.; Ohashi, M.; Kaneko, T.; Yuzuri, M.; Yamaguchi, Y.; Funahashi, S.; Morii, Y. Magnetic structure of rhombohedral Cr_2Se_3. *J. Phys. Soc. Jpn.* **1994**, *63*, 1548−1559.
(34) Andresen, A. F.; et al. The magnetic structure of Cr_2Te_3, Cr_3Te_4, and Cr_5Te_6. *Acta Chem. Scand.* **1970**, *24*, 3495−3509.
(35) Horton, M. K.; Montoya, J. H.; Liu, M.; Persson, K. A. High-throughput prediction of the ground-state collinear magnetic order of inorganic materials using Density Functional Theory. *npj Comp. Mater.* **2019**, *5*, 64.
(36) Spaldin, N. A. Magnetic Materials: Fundamentals and Applications. *MRS Bull.* **2017**, *42*, 385−390.
(37) Morosan, E.; Zandbergen, H. W.; Dennis, B. S.; Bos, J. W. G.; Onose, Y.; Klimczuk, T.; Ramirez, A. P.; Ong, N. P.; Cava, R. J. Superconductivity in $CuxTiSe_2$. *Nat. Phys.* **2006**, *2*, 544−550.
(38) Nair, N. L.; Maniv, E.; John, C.; Doyle, S.; Orenstein, J.; Analytis, J. G. Electrical switching in a magnetically intercalated transition metal dichalcogenide. *Nat. Mater.* **2020**, *19*, 153−157.
(39) Hatanaka, T.; Nomoto, T.; Arita, R. Magnetic interactions in intercalated transition metal dichalcogenides: A study based on ab initio model construction. *Phys. Rev. B* **2023**, *107*, 184429.

https://doi.org/10.1021/acs.nanolett.3c03169
Nano Lett. 2023, 23, 9579−9586